JACS
JOURNAL OF THE AMERICAN CHEMICAL SOCIETY

ARTICLE

pubs.acs.org/JACS

Charge Delocalization in a Cyclometalated Bisruthenium Complex Bridged by a Noninnocent 1,2,4,5-Tetra(2-pyridyl)benzene Ligand

Chang-Jiang Yao, Yu-Wu Zhong,* and Jiannian Yao*

Beijing National Laboratory for Molecular Sciences, CAS Key Laboratory of Photochemistry, Institute of Chemistry, Chinese Academy of Sciences, Beijing 100190, People's Republic of China

Supporting Information

ABSTRACT: Two ruthenium atoms are covalently connected to the para positions of a phenyl ring in 1,2,4,5-tetra(2-pyridyl)-benzene (tpb) to form a linear Ru−tpb−Ru arrangement. This unique structure leads to appealing electronic properties for the biscyclometalated complex $[(tpy)Ru(tpb)Ru(tpy)]^{2+}$, where tpy is 2,2′;6′,2″-terpyridine. It could be stepwise oxidized at substantially low potential (+0.12 and +0.55 V vs Ag/AgCl) and with a noticeably large comproportionation constant (1.94×10^7). In addition to the routinely observed metal-to-ligand charge-transfer transitions, $[(tpy)Ru(tpb)Ru(tpy)]^{2+}$ displays a separate and distinct absorption band at 805 nm with appreciable absorptivity ($\varepsilon = 9000\ M^{-1}\ cm^{-1}$). This band is assigned to the charge transition from the Ru−tpb−Ru motif to the pyridine rings of tpb with the aide of density functional theory (DFT) and time-dependent DFT calculations. Complex $[(tpy)Ru(tpb)Ru(tpy)]^{2+}$ was precisely titrated with 1 equiv of cerium ammonium nitrate to produce $[(tpy)Ru(tpb)Ru(tpy)]^{3+}$, which shows intense multiple NIR transitions. The electronic coupling parameters H_{ab} of individual NIR components are determined to be 5812, 4942, 4358, and 3560 cm^{-1}. DFT and TDDFT calculation were performed on $[(tpy)Ru(tpb)Ru(tpy)]^{3+}$ to elucidate its electronic structure and spin density population and the nature of the observed NIR transitions. Electron paramagnetic resonance studies of $[(tpy)Ru(tpb)Ru(tpy)]^{3+}$ exhibit a discernible rhombic signal with the isotropic g factor of $\langle g \rangle = 2.144$. These results point to the strong orbital interaction of tpb with metal centers and that tpb behaves as a redox noninnocent bridging ligand in $[(tpy)Ru(tpb)Ru(tpy)]^{2+}$. Complex $[(tpy)Ru(tpb)Ru(tpy)]^{3+}$ is determined to be a Robin−Day class III system with full charge delocalization across the Ru−tpb−Ru motif.

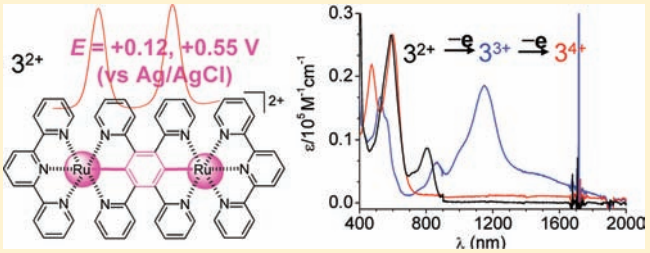

INTRODUCTION

The understanding of charge delocalization in conjugated compounds is of particular importance in designing and developing new semiconductor materials for optoelectronic applications.[1] In this regard, mixed-valence (MV) systems, with purely organic or organometallic components, have attracted growing interest since they provide simple models for the investigation of basic charge delocalization and electron transfer processes.[2] One of the most appealing motives in studying MV systems is that their charge delocalization degree could be qualitatively and quantitatively assessed by a combination of electrochemical and spectroscopic techniques. As demonstrated by enormous experimental data and sophisticated theoretical calculations,[2] the charge delocalization of MV systems greatly depends on a number of factors, such as the distance between redox centers, coordination environments of the metal components, and ability of the bridging ligand to delocalize the electronic charge. These studies are of significant importance in understanding many naturally occurring photoinduced electron/energy transfer processes and relevance to molecular electronics and switches. Despite these efforts, design and realization of new MV systems with full charge delocalization is still challenging.[3]

According to Robin and Day,[4] three categories of MV systems are distinguished on the basis of the extent of electronic coupling between individual redox centers. Class I systems are composed of noninteracting centers. Species in Class II systems exhibit weak or moderate coupling between individual redox components. Class III systems consist of strongly coupled centers in which electrons fully delocalize across the whole molecule and electron transfer between redox sites take places without an activation barrier. Among them, linear class III systems with full charge delocalization would be very attractive for applications in molecular electronics.[5] However, most MV complexes reported to date are classified as the class II system.

Polyazine transition-metal complexes are very useful and interesting for building MV systems.[6] These complexes often exhibit rich photophysical properties and multiple well-defined redox processes. Construction and investigations of linear polyazine multimetallic complexes have been the focus for several decades and recently gained renewed interest due to their potential use in molecular electronics.[7] We are particularly interested in construction of new MV systems with cyclometalated polyazine

Received: June 24, 2011
Published: August 24, 2011

Chart 1. Pyrazine- vs 1,4-Benzene-Bridged Mixed-Valent Bisruthenium Complexes[a]

[a]The counteranions and ancillary ligands are omitted.

Scheme 1. Synthesis of Compounds 1−3

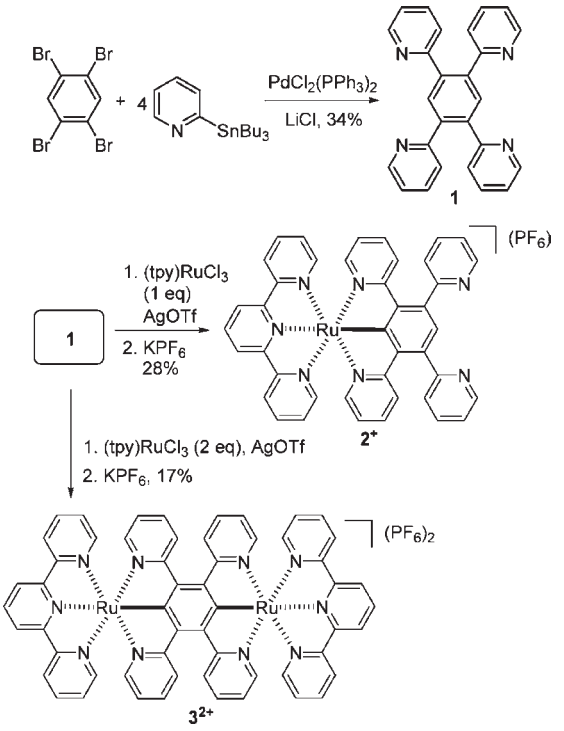

ruthenium complexes.[8] The anionic nature of the cyclometalating ligand significantly changes the properties of these complexes.[9] They have been reported to greatly enhance metal−metal coupling in MV systems,[10] as compared to noncyclometalated ones. In addition, cyclometalated ruthenium complexes have been used as efficient sensitizers for solar cell applications in numerous recent research activities.[11]

Complexes with redox noninnocent ligands, either ancillary or bridging ligands, show appealing and unique electronic properties and have been the focus of a number of research groups.[12] According to the definition by Jørgensen, a ligand is called noninnocent if it does not allow the oxidation state of the metal to be defined.[13] Two types of noninnocent ligands are well known. One class is 1,2-dioxolene, 1,2-dithiolene, *o*-phenylene diamine, and other electronically similar ligands.[14] Another is the anionic carbon ligand, such as phenylacetylene, phenylvinylene, or the phenyl group when covalently connected to a metal center.[15] Depending on the nature of the ligands and metals, redox processes of complexes with noninnocent ligands could occur from the ligand motif or the metal center or both components. For interpretation of the MV state of multimetallic complexes with noninnocent ligands, which show extended conjugation across the molecule, a combination of electrochemical, spectroscopic, magnetic, and theoretical analysis must be invoked.

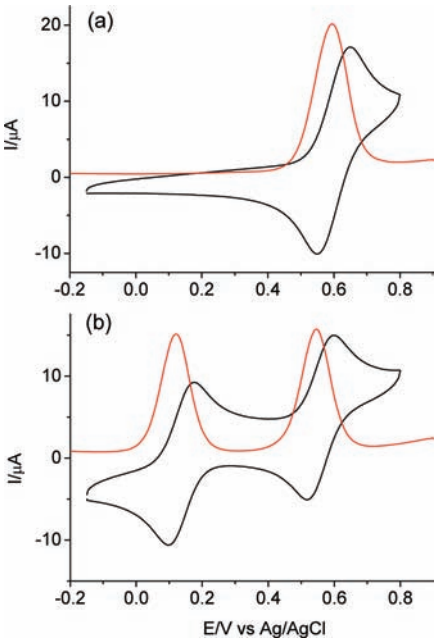

Figure 1. Cyclic voltammograms (CV, black lines) of (a) 2^+ and (b) 3^{2+} in acetonitrile containing 0.1 M $^nBu_4NClO_4$ at a scan rate of 100 mV/s. The red lines are differential pulse voltammograms with a step potential of 5 mV and an amplitude of 50 mV. The working electrode is glassy carbon, the counter electrode is a Pt wire, and the reference electrode is Ag/AgCl in saturated aq. NaCl. For CV profiles with wider potential windows, see Figures S1 and S2 in the Supporting Information.

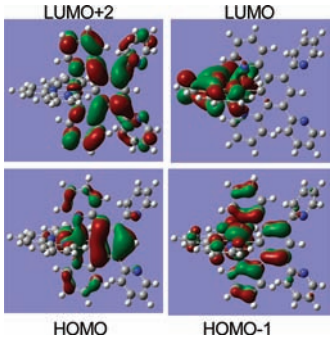

Figure 2. Isodensity plots of selected HOMO and LUMO orbitals for complex 2^+. All orbitals have been computed at an isovalue of 0.02.

We report in this article on new cyclometalated bisruthenium complexes $[(tpy)Ru(tpb)Ru(tpy)]^{2+}$ and the one-electron oxidized species $[(tpy)Ru(tpb)Ru(tpy)]^{3+}$, where tpy is 2,2′;6′,2″-terpyridine and tpb is the bridging 1,2,4,5-tetra(2-pyridyl)-benzene (tpb) ligand. In contrast to the familiar Cruetz−Taube ion bridged by a pyrazine ligand with dative bonds,[16] namely, $\{[Ru(NH_3)_5](pyrazine)[Ru(NH_3)_5]^{5+}\}$, ruthenium atoms in $[(tpy)Ru(tpb)Ru(tpy)]^{2+}$ and $[(tpy)Ru(tpb)Ru(tpy)]^{3+}$ are connected to the bridging ligand through covalent Ru−C bonds (Chart 1). Interestingly, complex $[(tpy)Ru(tpb)Ru(tpy)]^{2+}$ shows peculiar and unique electronic properties that have rarely been reported in other polyazine transition metal complexes, as revealed by detailed electrochemical, spectroscopic, and theoretical

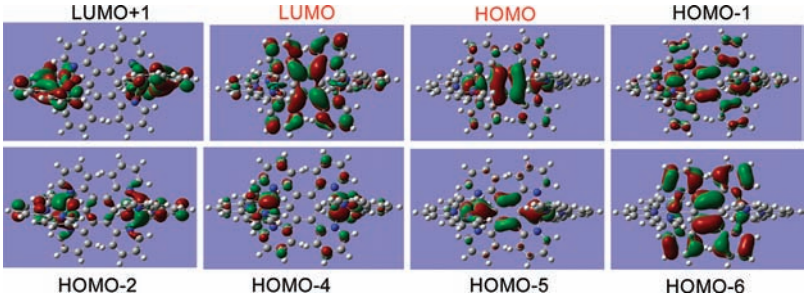

Figure 3. Isodensity plots of selected HOMO and LUMO orbitals for complex 3^{2+}. All orbitals have been computed at an isovalue of 0.02.

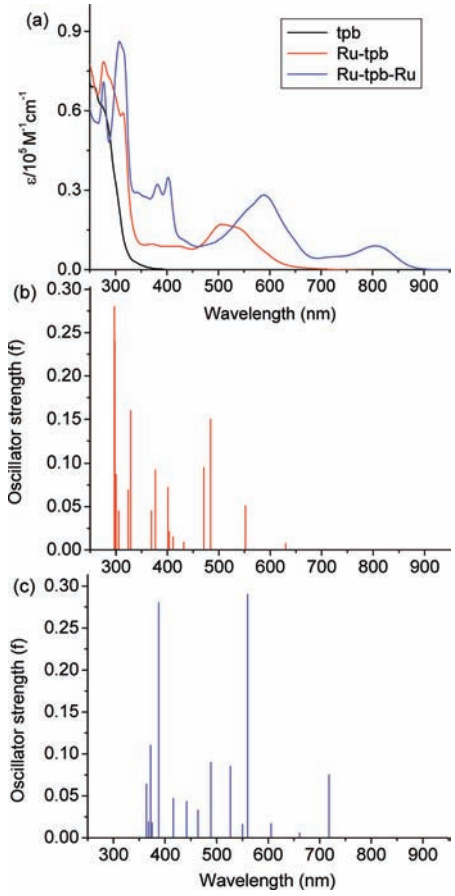

Figure 4. (a) Electronic absorption spectra of tpb **1** in dichloromethane (black line) and complexes 2^+ (red line) and 3^{2+} (blue line) in acetonitrile. (b and c) First 100 absorptions with oscillator strength values higher than 0.005 as predicted by TDDFT for complexes 2^+ and 3^{2+}, respectively.

calculation studies. In addition, strong electronic coupling was found to be present between individual redox centers as investigated on complex $[(tpy)Ru(tpb)Ru(tpy)]^{3+}$ with electrochemical and electron paramagnetic resonance (EPR) studies and by analyzing near-infrared transitions with the aide of theoretical calculations.

RESULTS AND DISCUSSION

Synthesis. As depicted in Scheme 1, tpb (**1**) was synthesized through the palladium-catalyzed Stille cross-coupling reaction[17] between 1,2,4,5-tetrabromobenzene and 2-(tributylstannyl)-pyridine in 34% yield. The reaction of 2 equiv of $(tpy)RuCl_3$ (tpy = 2,2′;6′,2″-terpyridine) with **1** in the presence of AgOTf, followed by subsequent counteranion exchange, afforded cyclometalated bisruthenium complex 3^{2+} in 17% yield. In addition, monoruthenium complex 2^+ was prepared from 1 equiv of $(tpy)RuCl_3$ with **1** for a comparison study. The identities of new compounds were confirmed by ^1H NMR, mass spectrometry, and microanalysis (see the Experimental Section for details).

Electrochemical Studies and DFT Calculations. Electrochemical techniques, such as cyclic voltammetric (CV) and differential pulse voltammetric (DPV) analysis, are frequently employed to study the electronic communication between metal centers of symmetric dimetallic systems. If no electronic coupling is present between two metals, the voltammetric profile exhibits a single metal-based redox wave. On the other hand, two separated sequential redox waves from the metals suggest the presence of an efficient charge delocalization between them. However, this principle should be taken with great care. Numerous studies[18] have proven that the electrochemical data are largely dependent on the measurement conditions, particularly the solvent and supporting electrolyte used. Nevertheless, the separation difference between two redox waves (ΔE^o) may serve as a parameter for qualitatively estimating the extent of electronic coupling between two metal centers if under the same conditions of measurement.

The anodic CV profile of monoruthenium complex 2^+ is shown in Figure 1a, which displays one reversible redox couple at +0.60 V vs Ag/AgCl. This is a typical value for a cyclometalated $Ru^{II/III}$ redox process.[8−11] On the other hand, two sequential redox couples at +0.12 and +0.55 V are evident on the CV of bisruthenium complex 3^{2+} (Figure 1b), with a potential difference (ΔE^o) of 430 mV between two half-wave potentials. Differential pulse voltammetry (DPV) of 3^{2+} (red line in Figure 1b) also confirms this result. Noteworthy is that both redox processes of 3^{2+} occur at less positive potentials than that of 2^+. This phenomenon is rarely observed in MV systems, because the redox process of the monometallic complex usually takes place at a potential between those of the two splitting waves of the homologous dimetallic complex. In addition, the first oxidation potential at +0.12 V vs Ag/AgCl of complex 3^{2+} is too low to be simply ascribed to a cyclometalated $Ru^{II/III}$ redox process.[9−11] We reason that attachment of two cyclometalated ruthenium atoms makes the anionic bridging ligand sufficiently electron rich to become noninnocent. In other words, the redox processes of 3^{2+} shown in Figure 1b are attributable to an admixture of oxidations from both the metal center and the bridging ligand. We notice that the electrochemical behaviors of 3^{2+} are in stark contrast with another biscyclometalated bisruthenium complex $[(tpy)Ru(dpdpz)Ru(tpy)](PF_6)_2$

Table 1. Excitation Energy (E), Oscillator Strength (f), Dominant Contributing Transitions, and Associated Percent Contribution and Assignment of Complex 2^{+a}

S_n	E/eV	E/nm	f	dominant transitions (percent contribution[b])	assignment[b]
3	1.97	630	0.0073	HOMO−1 → LUMO (74%)	$ML_{tpy}CT$
5	2.24	552	0.051	HOMO−2 → LUMO+1 (87%)	$ML_{tpy}CT$
6	2.56	484	0.15	HOMO−2 → LUMO (39%)	$ML_{tpy}CT$
				HOMO−1 → LUMO+1 (30%)	$ML_{tpy}CT$
7	2.63	471	0.095	HOMO → LUMO+2 (84%)	$ML_{tpb}CT/IL_{tpb}CT$
9	2.87	432	0.0088	HOMO → LUMO+3 (56%)	$ML_{tpb}CT/IL_{tpb}CT$
				HOMO−1 → LUMO+2 (34%)	$ML_{tpb}CT$
13	3.02	411	0.015	HOMO−2 → LUMO+3 (63%)	$ML_{tpb}CT$
15	3.09	401	0.072	HOMO−1 → LUMO+3 (84%)	$ML_{tpb}CT$
19	3.29	377	0.092	HOMO−1 → LUMO+4 (61%)	$ML_{tpy}CT$
21	3.36	369	0.045	HOMO−1 → LUMO+5 (50%)	$ML_{tpy}CT$
33	3.77	329	0.16	HOMO−3 → LUMO+2 (56%)	IL_{tpb}
				HOMO−5 → LUMO+2 (27%)	IL_{tpb}
36	3.82	324	0.069	HOMO−5 → LUMO+2 (61%)	IL_{tpb}
47	4.06	305	0.045	HOMO−2 → LUMO+14 (52%)	M_c
48	4.13	300	0.055	HOMO−2 → LUMO+8 (41%)	$ML_{tpy}CT$
49	4.13	300	0.087	HOMO → LUMO+10 (61%)	IL_{tpb}
51	4.16	298	0.24	HOMO−6 → LUMO+2 (37%)	IL_{tpb}
				HOMO → LUMO+10 (30%)	IL_{tpb}
52	4.17	297	0.28	HOMO−9 → LUMO (72%)	IL_{tpy}

[a] Computed at the TDDFT/LANL2DZ level of theory. [b] The actual percent contribution = (configuration coefficient)^2 × 2 × 100%.

reported by us recently,[8a] where dpdpz is 2,3-di(2-pyridyl)-5,6-diphenylpyrazine and the metal center binds to the bridging ligand in a tridentate C^N^N fashion. The first two oxidation processes of this complex take place at +0.65 and +0.84 V vs Ag/AgCl. This suggests the position of the Ru−C bond plays a significant role in determining the electronic properties of biscyclometalated ruthenium complexes. The tridentate N^C^N coordination mode with the bridging tpb ligand in complex 3^{2+} is essential for its peculiar properties.

Density functional theory (DFT) calculations were performed on the B3LYP/LANL2DZ level to assist determination of their electronic structures. Selected frontier orbital structures of 2^+ and 3^{2+} with electron density distributions are shown in Figures 2 and 3, respectively. More orbital graphics can be found in Figures S3−S6 in the Supporting Information. The lowest unoccupied molecular orbital (LUMO) and LUMO+1, LUMO+4, LUMO +5, and LUMO+8 of 2^+ have major contributions from the ancillary tpy ligand, while LUMO+2, LUMO+3, and LUMO+10 are dominated by the tpb ligand. In addition, the ruthenium component contributes dominantly to LUMO+14. The highest occupied molecular orbital (HOMO) of 2^+ has contributions from both the metal component and the center phenyl ring of tpb ligand. Mulliken population analysis of the HOMO composition reveals a value of 0.48 and 0.34 for the metal center and the cyclometalating phenyl fragment. HOMO-1 and HOMO-2 are dominated by the metal component. As for the lower occupied orbitals, HOMO-3, HOMO-5, and HOMO-6 have a major contribution from the tpb ligand while HOMO-9 is dominated by the ancillary tpy ligand. Interestingly, the situation is significantly different in the case of bisruthenium complex 3^{2+}. The bridging tpb ligand, instead of tpy, contributes dominantly in the LUMO of 3^{2+}. Higher unoccupied orbitals have a major contribution from either tpy (LUMO+1, LUMO+2, LUMO+3, and LUMO+4), tpb (LUMO+5 and LUMO+14), or the metal center (LUMO+9). The electron density of the HOMO of 3^{2+} distributes across the Ru−tpb−Ru motif, with tpb even playing a more important role. The Mulliken population of the cyclometalating phenyl fragment is 0.29, which is larger than that of each metal center (0.25). This supports the above electrochemical results that a considerable portion of oxidation processes of 3^{2+} may arise from the bridging tpb component.

Electronic Absorption Spectra and TDDFT Calculations. To further probe the electronic properties of complexes 2^+ and 3^{2+}, their electronic absorption spectra were subsequently recorded (Figure 4a). To aid in the assignment of the optical absorptions more precisely, the nature of the low-energy transitions was studied by time-dependent DFT (TDDFT) calculations. The first 100 predicted transitions of complexes 2^+ and 3^{2+} are shown in Figure 4b and 4c, respectively. Tables 1 and 2 give major predicted transitions with the excitation energy (E), oscillator strength (f), dominant configuration contribution, and assignment. Monoruthenium complex 2^+ displays multiple sharp and intense excitations below 350 nm and a broad transition between 450 and 650 nm. According to TDDFT predications (Figure 4b and Table 1) and in agreement with previous assignment for similar cyclometalated ruthenium complexes,[8−11] absorptions in the UV region are ascribed to intraligand (IL) $\pi-\pi^*$ transitions of both tpy and tpb ligands mixed with a small portion of a metal-centered transition. The relatively shallow absorptions between 350 and 450 nm are attributable to an admixture of metal-to-ligand charge-transfer (MLCT) transitions from ruthenium to both tpy and tpb ligands. The broad transition centered at 500 nm has major contribution from $ML_{tpy}CT$ transition (excitations from HOMO-1 and HOMO-2 to LUMO and LUMO+1) mixed with some $ML_{tpb}CT$ transition and $IL_{tpb}CT$ (intramolecular charge-transfer) transitions. The latter two transitions are due to excitation from HOMO to LUMO-2 and LUMO-3, respectively.

Table 2. Excitation Energy (E), Oscillator Strength (f), Dominant Contributing Transitions, and Associated Percent Contribution and Assignment of Complex 3^{2+a}

S_n	E/eV	E/nm	f	dominant transitions (percent contribution[b])	assignment[b]
3	1.72	718	0.075	HOMO → LUMO (85%)	CT(Ru−tpb−Ru → L_{tpb})
5	1.88	661	0.0056	HOMO → LUMO+4 (92%)	CT(Ru−tpb−Ru → L_{tpy})
6	2.05	606	0.017	HOMO−1 → LUMO+1 (56%)	$ML_{tpy}CT$
9	2.21	560	0.29	HOMO−1 → LUMO (85%)	$ML_{tpb}CT$
14	2.35	527	0.085	HOMO−2 → LUMO+4 (48%)	$ML_{tpy}CT$
				HOMO−3 → LUMO+3 (39%)	$ML_{tpy}CT$
17	2.53	489	0.090	HOMO → LUMO+5 (65%)	CT(Ru−tpb−Ru → L_{tpb})
21	2.67	464	0.033	HOMO−5 → LUMO+1 (27%)	$ML_{tpy}CT$
				HOMO−1 → LUMO+4 (23%)	$ML_{tpy}CT$
33	2.81	442	0.043	HOMO−4 → LUMO+3 (67%)	$ML_{tpy}CT$
38	2.98	416	0.047	HOMO−1 → LUMO+5 (77%)	$ML_{tpb}CT$
43	3.19	388	0.28	HOMO−1 → LUMO (65%)	$ML_{tpb}CT$
49	3.30	375	0.018	HOMO−2 → LUMO+9 (50%)	M_c
53	3.33	372	0.11	HOMO−1 → LUMO+9 (65%)	M_c
55	3.37	368	0.019	HOMO → LUMO+14 (65%)	IL_{tpb}
57	3.40	364	0.064	HOMO−6 → LUMO+4 (90%)	$L_{tpb}L_{tpy}CT$

[a] Computed at the TDDFT/LANL2DZ level of theory. [b] The actual percent contribution = (configuration coefficient)^2 × 2 × 100%.

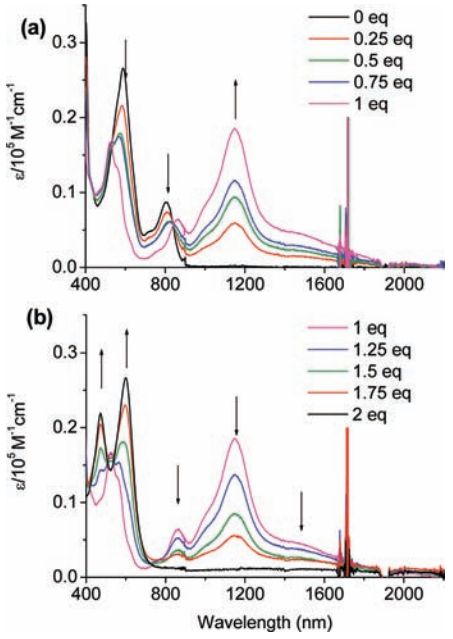

Figure 5. Absorption spectral changes of bisruthenium complex 3^{2+} in acetonitrile upon one-electron (a) and two-electron (b) oxidation by adding different equivalents of cerium ammonium nitrate (up to 2 equiv) while keeping the concentration of 3^{2+} constant. The irregular peaks at 1700 nm are due to artifacts.

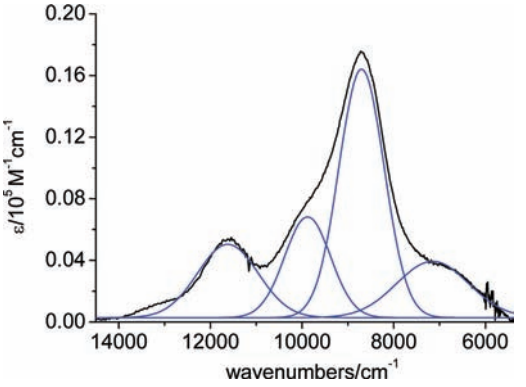

Figure 6. Deconvolution of the NIR spectra of 3^{3+} generated by adding 1 equiv of cerium ammonium nitrate in acetonitrile. See text for details. Irregular noises at 6000 cm^{-1} were deleted intentionally before deconvolution.

In comparison, the IL and MLCT transitions of 3^{2+} shift bathochromically and their absorptivity increases considerably. However, the most striking absorption feature of 3^{2+} is the emergence of a separate new band at 805 nm. This kind of spectrum is reminiscent of absorption of polyazine osmium complexes, which often display ^{3}MLCT transitions at a lower energy region in addition to ^{1}MLCT transitions in the visible region. However, ^{3}MLCT electronic transitions have never been documented, to the best of our knowledge, in the case of polyazine ruthenium complexes at room temperature. This is because the spin−orbit coupling effect of ruthenium is not as heavy as that of osmium. Taking into account the unusual observation in the electrochemical analysis of 3^{2+} and the TDDFT prediction of the presence of a low-energy transition at 718 nm from the HOMO → LUMO excitation (f = 0.075), we assign the observed absorption at 805 nm mainly to the CT transition from the Ru−tpb−Ru component to the pyridine rings of tpb ligand.

NIR Transition Analysis of Mixed-Valence Species. As is clear from the above discussion, the bridging ligand in complex 3^{2+} is redox noninnocent. Thus, one-electron-oxidized intermediate 3^{3+} could not be described as a true MV system with defined metal oxidation state. Nevertheless, the comproportionation constant K_c could be determined to be 1.94 × 10^7 by the equation $K_c = 10^{\Delta E\ (\mathrm{mV})/59}$ for a room-temperature case,[2] where ΔE is the potential splitting observed in Figure 1b (430 mV). The substantially large K_c value indicates the high thermodynamic

Table 3. Parameters for the Deconvoluted NIR Transitions of 3^{3+}

λ_{max}/nm	ν_{max}/cm^{-1}	ε_{max} (M^{-1} cm^{-1})	$\Delta\nu_{1/2}$(exp) (cm^{-1})	$\Delta\nu_{1/2}$(theor)[a] (cm^{-1})	Γ[b]	H_{ab}[c] (cm^{-1})
860	11624	5100	1560	5181	0.70	5812
1012	9884	6800	1160	4778	0.76	4942
1147	8717	16500	1160	4487	0.74	4358
1405	7120	3950	1850	4055	0.54	3560

[a] The theoretical $\Delta\nu_{1/2}$ value equals $(2310\nu_{max})^{1/2}$. [b] $\Gamma = 1 - \Delta\nu_{1/2exp}/\Delta\nu_{1/2theo}$. [c] $H_{ab} = 1/2\ \nu_{max}$ for a Robin and Day class III system.

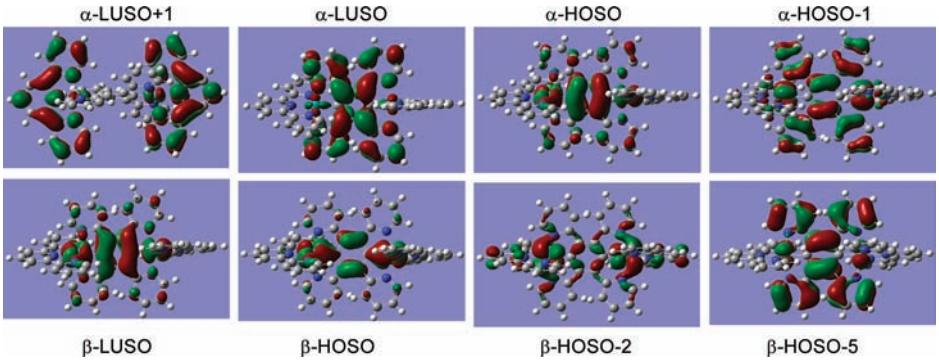

Figure 7. Isodensity plots of selected HOSO and LUSO orbitals for complex 3^{3+}. All orbitals have been computed at an isovalue of 0.02.

Table 4. Calculated Spin Density Distribution of Complex 3^{3+} on the Level of B3LYP/LanL2DZ/6-31G*[a]

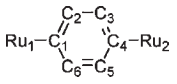

atom	spin density	atom	spin density
Ru_1	0.326	C_3	0.043
Ru_2	0.326	C_4	0.050
C_1	0.050	C_5	0.043
C_2	0.043	C_6	0.043

[a] Spin density is determined by the difference of the Mulliken charges of α and β electrons $(\alpha - \beta)$.

stability of the in-situ-generated one-electron-oxidized MV intermediate. This allows us to precisely titrate 3^{2+} with 1 or 2 equiv of oxidant, cerium ammonium nitrate (CAN), and monitor corresponding vis/NIR absorption spectral changes (Figure 5). When a solution of 3^{2+} in acetonitrile was gradually treated with 0.25−1 equiv of CAN, both charge-transfer transitions at 588 and 805 nm decrease continually and substantially. At the same time, the emergence of multiple overlapping bands between 800 and 2000 nm is evident. When the amount of CAN was gradually increased to 2 equiv, two new peaks at 470 and 600 nm appear, meanwhile all transitions in the near-infrared (NIR) region decrease gradually until they disappear completely. The former two peaks could be assigned to the charge-transfer transitions from the tpy and the tpb ligand to the oxidized Ru−tpb−Ru motif, and the multiple NIR peaks are associated with the MV system 3^{3+}. By assuming Gaussian shapes, the NIR transitions could be at least deconvoluted into four distinct bands at 860, 1012, 1147, and 1405 nm (Figure 6). Corresponding parameters and analysis of these NIR bands are collected in Table 3. All of these bands are remarkably narrow, with the observed full width at half-height ($\Delta\nu_{1/2}$) of 1560, 1160, 1160, and 1850 cm^{-1}, respectively. The theoretical $\Delta\nu_{1/2}$ values of these bands were determined to be 5181, 4778, 4487, and 4055 cm^{-1}, respectively, according to Hush's expression $(\Delta\nu_{1/2theor} = (2310\nu_{max})^{1/2})$.[19] It is clear that the experimental values of $\Delta\nu_{1/2}$ are much narrower than the theoretical ones. The Γ parameters, introduced by Creutz, Sutin, and co-workers,[20] of these bands are all bigger than 0.5 (0.70, 0.76, 0.74, and 0.54, respectively), as determined by $\Gamma = 1 - \Delta\nu_{1/2exp}/\Delta\nu_{1/2theor}$. On the basis of these facts and taking into account the peculiar results observed in the electrochemical, spectroscopic, and DFT/TDDFT analysis, we conclude that 3^{3+} is a Robin and Day class III system. The electronic coupling parameter H_{ab} is thus calculated to be 5812, 4942, 4358, and 3560 cm^{-1}, respectively, for the above four observed NIR bands, according to the equation $H_{ab} = 1/2\nu_{max}$ for a Robin and Day class III system. It should be noted here that the observed NIR bands for a class III system are more correctly described as charge-resonance bands rather than intervalence charge-transfer (IVCT) transitions.

Observation of multiple NIR bands for MV system 3^{3+} deserves further comment. The presence of multiple IVCT bands in the spectrum of a MV system is not an uncommon occurrence, though they are not routinely observed. For instance, a mixed-valent diaza[2,2]ferrocenophane compound exhibits two IVCT bands associated with two different stable conformers present in the system.[21] A number of bisosmium MV complexes have been reported to display up to five IVCT bands due to the strong spin−orbit coupling effect of the osmium atom.[22] However, as for ruthenium complexes, only a few MV systems disclose the observation of multiple NIR transitions. For example, complexes $\{[Cl_3Ru^{II}(tppz)Ru^{III}Cl_3]^-\}$[23] and $\{[Ru(NH_3)_5](bqd)[Ru(NH_3)_5]^{5+}\}$,[24] where tppz is 2,3,5,6-tetrakis(2-pyridyl)pyrazine and bqd is *p*-benzoquinone diimine, have been reported to show multiple IVCT transitions. Complex 3^{3+} represents another new

Table 5. Calculated Low-Energy Excitations of Complex 3^{3+}

method	S_n	E/eV	E/nm	f	dominant transitions (configuration coefficient)
B3LYP/LanL2DZ/6-31G*/vacuum	2	0.87	1418	0.0075	β-HOSO-2 → β-LUSO (0.95)
	5	1.07	1157	0.2314	β-HOSO → β-LUSO (0.95)
	6	1.65	749	0.0023	β-HOSO-5 → β-LUSO (0.97)
	7	1.91	647	0.054	α-HOSO → α-LUSO (0.98)
	33	2.69	460	0.185	α-HOSO-1 → α-LUSO (0.62)
B3LYP/LanL2DZ/6-31G*/ CPCM(CH_3CN)	2	0.89	1393	0.0152	β-HOSO-2 → β-LUSO (0.93)
	4	0.99	1245	0.0012	β-HOSO-3 → β-LUSO (0.99)
	5	1.05	1179	0.2905	β-HOSO → β-LUSO (0.95)
	6	1.66	748	0.0032	β-HOSO-5 → β-LUSO (0.97)
B3LYP/SDD/6-31G*/ CPCM(CH_3CN)	2	0.88	1411	0.0168	β-HOSO-2 → β-LUSO (0.91)
	4	0.98	1269	0.0013	β-HOSO-3 → β-LUSO (0.99)
	5	1.05	1178	0.2931	β-HOSO → β-LUSO (0.94)
	6	1.71	724	0.0031	β-HOSO-5 → β-LUSO (0.97)

MV system with multiple discernible NIR bands with high intensity. We reason that in the case of complex 3^{3+} it is a result of the strong orbital interaction of the biscyclometalating bridging tpb ligand with the metal center and considerable participation of tpb into the oxidation process.

Given the redox noninnocent nature of the bridging ligand, it is somewhat ambiguous to analyze 3^{3+} on the basis of the classical Hush theory and the Robin−Day classification, which are best applicable to systems with well-defined redox centers. Thus, we performed DFT and TDDFT calculations of complex 3^{3+} to further elucidate the nature of its electronic structure and the observed NIR transitions. DFT and TDDFT calculations have proven useful in the interpretation of organometallic systems with redox noninnocent ligands.[15e,25] DFT calculations for complex 3^{3+} were performed at the UB3LYP level with the LanL2DZ basis set for ruthenium and 6-31G* for other atoms in vacuum. TDDFT calculations were carried out on the DFT-optimized structure at the same UB3LYP/LanL2DZ/6-31G* level. Two Ru−C bonds in the DFT-optimized structure of 3^{3+} have identical length (1.954 Å). Compared with complex 3^{2+}, the Ru−C bond of the one-electron-oxidized 3^{3+} is shortened by 0.041 Å. However, all Ru−N bonds are lengthened by 0.04−0.05 Å. Some selected α- and β-spin frontier orbitals of 3^{3+} are shown in Figure 7. Most of them have very similar composition to the frontier orbitals described for complex 3^{2+} (Figure 3), albeit with a small change in relative ordering. For example, the electronic configurations of α-LUSO (lowest unoccupied spin orbital), α-HOSO (highest occupied spin orbital), α-HOSO-1, β-LUSO, β-HOSO, and β-HOSO-2 of MV complex 3^{3+} are very similar to LUMO, HOMO, HOMO-1, HOMO, HOMO-5, and HOMO-2 of complex 3^{2+}, respectively. The Mulliken spin density population analysis of complex 3^{3+} is summarized in Table 4. Two ruthenium atoms have identical spin density (0.326 each), which is in agreement with the Robin−Day class III assignment for 3^{3+}. A significant portion of spin resides in the cyclometalating phenyl ring (a total of 0.272), pointing to a strong electron delocalization across the Ru−dpb−Ru array. This is also corroborated by EPR analysis presented below.

Table 5 presents the calculated low-energy excitations of 3^{3+} with oscillator strength (f) larger than 0.001. The two lowest energy transitions (S_2 at 1418 nm and S_5 at 1157 nm) are in good agreement with the experimentally observed bands at 1405 and 1147 nm in terms of both energy and strength. They are mainly

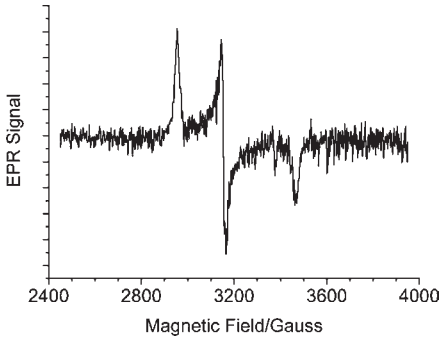

Figure 8. EPR signal of 3^{3+} at 77 K in acetonitrile. Spectrometer frequency ν is 9.519×10^9 Hz.

associated with excitation of a β electron to β-LUSO from β-HOSO-2 and β-HOSO levels, respectively. These transitions could be interpreted as the charge-transfer transition from the metal centers to the bridging phenyl ring. It is important to note that β-HOSO-2 and β-HOSO levels have different metal orbital configurations (d_{xz} and d_{xy}, respectively), which could be partially responsible for the observation of multiple NIR bands. TDDFT calculations do not well predict the bands at 1012 and 860 nm. However, the band at 860 nm may have some LMCT character, since a β-HOSO-5 → β-LUSO transition at 749 nm is predicted by TDDFT results. In addition, the observed band at 524 nm could be assigned to a MLCT transition associated with α-HOSO-1 → α-LUSO excitation. Since the above TDDFT results did not predict the origin of the shoulder peak at 1012 nm, we performed new DFT and TDDFT calculations with inclusion of solvation effects in acetonitrile using the conductor-like polarizable continuum model (CPCM).[26] However, very similar results were obtained as those calculated in vacuum (table 5). When the SDD basis set[27] with effective core potential was employed for the ruthenium atom in combination CPCM (table 5), TDDFT calculations still cannot predict the peak at 1012 nm. It seems that TDDFT calculations could not fully agree with the experimentally observed NIR transitions of complex 3^{3+} and new calculation methods are desirable in the future. Nevertheless, TDDFT results predict well the major band at 1147 nm and provide instructive information regarding the charge resonance of complex 3^{3+}.

EPR Studies. The strong metal−metal coupling in $\mathbf{3}^{3+}$ is also supported by EPR studies. Complex $\mathbf{3}^{3+}$, obtained after one-electron oxidation of $\mathbf{3}^{2+}$ by adding 1 equiv CAN, is EPR silent at room temperature. However, it exhibits a rhombic EPR signal at 77 K typical for a low-spin Ru^{III} species (Figure 8). The electron g factors g_1, g_2, and g_3 are 2.302, 2.156, and 1.962, respectively. The isotropic g factor of $\langle g\rangle = 2.144$, derived according to $\langle g\rangle = [(g_1^2 + g_2^2 + g_3^2)/3]^{1/2}$. The total g anisotropy $\Delta g = g_1 - g_3 = 0.34$. The isotropic g factor of $\mathbf{3}^{3+}$ is much lower than those for the Cruetz−Taube ion (2.298)[28] and a bisruthenium Robin−Day class III system bridged by 3,6-bis(2-pyridyl)-1,2,4,5-tetrazine (2.477).[29] We also notice that a true metal-centered spin of a cetecholatoruthenium(III) complex has a $\langle g\rangle$ value of 2.476 with $\Delta g = 0.833$.[30] The pronounced rhombicity of the EPR signal and substantial low $\langle g\rangle$ and Δg values of complex $\mathbf{3}^{3+}$ points to a significant participation of ligand oxidation. This is in agreement with the spin density population analysis and experimental findings observed in the electrochemical and spectroscopic studies.

CONCLUSION

To summarize, we present in this contribution a new biscyclometalated bisruthenium complex $[(tpy)Ru(tpb)Ru(tpy)]^{2+}$ and its one-electron-oxidized species $[(tpy)Ru(tpb)Ru(tpy)]^{3+}$ bridged by 1,2,4,5-tetra(2-pyridyl)benzene. A combination of electrochemical, spectroscopic, DFT/TDDFT calculation, and EPR studies implies that tpb behaves as a redox noninnocent bridging ligand when coupled to two ruthenium atoms via covalent Ru−C bonds and the MV complex $[(tpy)Ru(tpb)Ru(tpy)]^{3+}$ is determined to be a Robin−Day class III system with full charge delocalization across the Ru−tpb−Ru motif. Complex $[(tpy)Ru(tpb)Ru(tpy)]^{2+}$ exhibits very peculiar and unique electronic properties that have not been commonly observed in most transition metal polyazine complexes. The electrochemical studies show that the first two oxidation processes take place at a substantially lower potential (+0.12 and +0.55 V vs Ag/AgCl) than common cyclometalated ruthenium complexes and with a remarkably large comproportionation constant (1.94×10^7). These features would allow us to readily access different oxidation states of $[(tpy)Ru(tpb)Ru(tpy)]^{2+}$ and facilitate realization of redox-controlled single-molecule conductance.[31] In addition, low oxidation potential and reversible redox process would make such compounds promising hole transporting materials for optoelectronic applications.[32] In terms of electronic absorption transitions, complex $[(tpy)Ru(tpb)Ru(tpy)]^{2+}$ distinguishes itself from other ruthenium polyzaine complexes as well. In addition to the routinely observed MLCT transitions in the visible region for those compounds, it displays a separate and distinct band on the lower energy side (805 nm) with appreciable absorptivity ($\varepsilon = 9000\ M^{-1}\ cm^{-1}$). This band is assigned to the charge transition from the Ru−tpb−Ru motif to the pyridine rings of tpb. Finally, observation of multiple NIR bands in the MV system $[(tpy)Ru(tpb)Ru(tpy)]^{3+}$ is worthy of particular attention. This represents one of the few examples of ruthenium MV complexes that display multiple NIR transitions. The strong orbital interaction of the biscyclometalating bridging ligand with the metal center and the significant participation of tpb into the oxidation processes is thought to be responsible for the appearance of multiple NIR transitions. According to TDDFT calculations, these bands are predominantly associated with the charge-transfer transition from the metal centers to the biscyclometalating phenyl ring. The high intensity of the NIR bands of $[(tpy)Ru(tpb)Ru(tpy)]^{3+}$, which are completely absent in $[(tpy)Ru(tpb)Ru(tpy)]^{2+}$ and the two-electron oxidized species $[(tpy)Ru(tpb)Ru(tpy)]^{4+}$, would make it a promising candidate as a NIR electrochromic material.[33] These appealing electronic properties of complexes $[(tpy)Ru(tpb)Ru(tpy)]^{2+}$ and $[(tpy)Ru(tpb)Ru(tpy)]^{3+}$ provide important guides for the design and synthesis of new MV systems with potential applications in molecular electronics, and construction of other MV complexes bridged by biscyclometalating ligands is underway in this laboratory.

EXPERIMENTAL SECTION

Spectroscopic Measurements. All optical ultraviolet−visible (UV−vis) absorption spectra were obtained using a TU-1810DSPC spectrometer of Beijing Purkinje General Instrument Co. Ltd. at room temperature in denoted solvents, with a conventional 1.0 cm quartz cell. UV−vis−NIR spectra were recorded using a JASCO V-570 UV/vis/NIR spectrophotometer.

Electrochemical Measurements. All cyclic voltammetry (CV) measurements were taken using a CHI620D potentiostat. All measurements were carried out in 0.1 M Bu_4NClO_4/acetonitrile at a scan rate of 100 mV/s with a Ag/AgCl reference electrode. The working electrode is a glassy carbon electrode, and a platinum coil is used as the counter electrode.

Computational Methods. DFT calculations are carried out using the B3LYP exchange correlation functional[34] and implemented in the Gaussian 03 program package.[35] The electronic structures of the complexes were determined using a general basis set with the Los Alamos effective core potential LanL2DZ or the SDD basis set for ruthenium and 6-31G* for other atoms in vacuum.[36] In case the solvation effects are included, the conductor-like polarizable continuum model (CPCM) with solvent = acetonitrile and united-atom Kohn−Sham (UAKS) radii were employed.[26]

Synthesis. NMR spectra were recorded in the designated solvent on a Bruker Avance 400 MHz spectrometer. Spectra are reported in ppm values from residual protons of deuterated solvent for ^1H NMR (δ 7.26 ppm for $CDCl_3$ and 1.92 ppm for CD_3CN) and ^{13}C NMR (δ 77.00 ppm for $CDCl_3$). MS data were obtained with a Bruker Daltonics Inc. ApexII FT-ICR or Autoflex III MALDI-TOF mass spectrometer. The matrix for MALDI-TOF measurement is α-cyano-4-hydroxycinnamic acid (CCA). Microanalysis was carried out using a Flash EA 1112 or Carlo Erba 1106 analyzer at the Institute of Chemistry, CAS.

Synthesis of 1. To a solution of 1,2,4,5-tetrabromobenzene (0.3 mmol, 118 mg) and 2-(tributylstannyl)pyridine (3.0 mmol, 1.1 g) in dry toluene (20 mL) were added $PdCl_2(PPh_3)_2$ (0.08 mmol, 56.1 mg) and anhydrous LiCl (6 mmol, 254 mg) under a N_2 atmosphere. The mixture was bubbled with nitrogen for 10 min before the vial was capped and heated at 150 °C for 48 h. The solvent was removed under reduced pressure, and the residue was subject to flash column chromatography on silica gel (eluent, CH_2Cl_2/ethyl acetate/NH_4OH 50/100/0.05) to afford 41 mg of **1** as a white solid. The yield is 34%. ^1H NMR (400 MHz, $CDCl_3$): δ 7.09 (dd, J = 11.4, 7.8 Hz, 4H), 7.13−7.15 (m, 4H), 7.45−7.49 (m, 4H), 8.06 (s, 2H), 8.60 (t, J = 4.2 Hz, 4H). ^{13}C NMR (100 MHz, $CDCl_3$): δ 122.3, 125.8, 133.4, 136.2, 140.4, 150.1, 159.2. ESI-MS (m/z): 387.3 for $[M + H]^+$. EI-HRMS (m/z): calcd 387.1610 for $C_{26}H_{19}N_4$ ($[M + H]^+$), found 387.1607.

Synthesis of [2](PF$_6$). To 50 mL of dry acetone were added $Ru(tpy)Cl_3$ (0.1 mmol, 44 mg) and AgOTf (0.3 mmol, 78 mg). The mixture was then refluxed under a N_2 atmosphere for 3 h. The mixture was filtered to afford a purple black solution, and the filtrate was concentrated to dryness. To the residue were added 1,2,4,5-tetra(pyridin-2-yl)benzene, **1** (0.1 mmol, 38.6 mg), 20 mL of DMF, and 20 mL of *t*-BuOH. The system was heated under microwave irradiation (375 W) for 30 min before cooling to room temperature. The solvent was removed under reduced pressure,

and the residue was dissolved in 3 mL of methanol. After adding an excess of KPF_6, the resulting precipitate was collected by filtering and washing with water and Et_2O. The crude solid was purified through flash column chromatography on silica gel followed by anion exchange with KPF_6 to give 24 mg of monoruthenium complex $[\mathbf{2}](PF_6)$ as a black solid (eluent, CH_3CN/H_2O/aq.KNO_3 100/5/0.03). The yield is 28%. ^{1}H NMR (400 MHz, $CDCl_3$): δ 6.57 (t, J = 6.4 Hz, 2H), 6.84 (d, J = 8.3 Hz, 2H), 7.06 (t, J = 5.6 Hz, 4H), 7.20 (t, J = 11.2 Hz, 3H), 7.30 (d, J = 5.0 Hz, 2H), 7.51 (t, J = 6.4 Hz, 2H), 7.72 (t, J = 7.6 Hz, 2H), 7.77 (d, J = 7.7 Hz, 2H), 7.97 (t, J = 7.6 Hz, 2H), 8.27 (t, J = 7.9 Hz, 1H), 8.44 (d, J = 8.0 Hz, 2H), 8.77 (t, J = 8.5 Hz, 2H). ESI-MS (m/z): 720.14 for $[M - PF_6]^+$. Anal. Calcd for $C_{41}H_{28}F_6N_7PRu$: C, 56.95; H, 3.26; N, 11.34. Found: C, 56.55; H, 3.73; N, 11.75.

Synthesis of [3](PF$_6$)$_2$. To 50 mL of dry acetone were added $Ru(tpy)Cl_3$ (0.1 mmol, 44 mg) and AgOTf (0.3 mmol, 78 mg). The mixture was then refluxed for 3 h. The mixture was filtered to afford a purple-black solution, and the filtrate was concentrated to dryness. To the residue were added 1,2,4,5-tetra(pyridin-2-yl)benzene, **1** (0.05 mmol, 19.3 mg), 20 mL of DMF, and 20 mL of *t*-BuOH. The mixture was bubbled with nitrogen for 10 min before the vial was capped and heated at 130 °C for 48 h. After cooling to room temperature, the solvent was removed under reduced pressure. The residue was then dissolved in 3 mL of methanol. After adding an excess of KPF_6, the resulting precipitate was collected by filtering and washing with water and Et_2O. The crude solid was purified through flash column chromatography on silica gel to give 11 mg of bisruthenium complex $[\mathbf{3}](PF_6)_2$ as a black solid. (eluent, CH_3CN/H_2O/aq.KNO_3 100/10/0.1). The yield is 17%. ^{1}H NMR (400 MHz, $CDCl_3$): δ 6.64 (s, 4H), 7.14 (s, 4H), 7.19 (d, J = 5.3 Hz, 4H), 7.51 (t, J = 7.7 Hz, 4H), 7.56 (d, J = 4.5 Hz, 4H), 7.79 (t, J = 7.6 Hz, 4H), 8.32 (t, J = 7.8 Hz, 2H), 8.41 (s, 4H), 8.52 (d, J = 8.0 Hz, 4H), 8.84 (d, J = 7.8 Hz, 4H). MALDI-MS (m/z): 1053.1 for $[M - 2PF_6 - H]^+$. Anal. Calcd for $C_{56}H_{38}F_{12}N_{10}P_2Ru_2 \cdot 2H_2O$: C, 48.77; H, 3.07; N, 10.16. Found: C, 48.64; H, 2.90; N, 10.34.

■ ASSOCIATED CONTENT

Supporting Information. CV profiles of $\mathbf{2}^+$ and $\mathbf{3}^{2+}$ with a wider potential window, selected frontier molecular orbital graphics of $\mathbf{2}^+$ and $\mathbf{3}^{2+}$, full list of authors of ref 35, and NMR and MS spectra of new compounds. This material is available free of charge via the Internet at http://pubs.acs.org.

■ AUTHOR INFORMATION

Corresponding Author

*Email: zhongyuwu@iccas.ac.cn (Y.-W.Z.); jnyao@iccas.ac.cn (J.Y.)

■ ACKNOWLEDGMENT

We thank the National Natural Science Foundation of China (No. 21002104), National Basic Research 973 program of China (Nos. 2011CB932301 and 2011CB808402), and Institute of Chemistry, Chinese Academy of Sciences ("100 Talent" Program) for funding support.

■ REFERENCES

(1) (a) Grimsdale, A. C.; Chan, K. L.; Martin, R. E.; Jokisz, P. G.; Holmes, A. B. *Chem. Rev.* **2009**, *109*, 897. (b) Szafert, S.; Gladysz, J. A. *Chem. Rev.* **2006**, *106*, PR1. (c) Tour, J. M. *Chem. Rev.* **1996**, *96*, 537. (d) Bunz, U. H. F. *Chem. Rev.* **2000**, *100*, 1605.

(2) (a) D'Alessandro, D. M.; Keene, F. R. *Chem. Rev.* **2006**, *106*, 2270. (b) Kaim, W.; Lahiri, G. K. *Angew. Chem., Int. Ed.* **2007**, *46*, 1778. (c) D'Alessandro, D. M.; Keene, F. R. *Chem. Soc. Rev.* **2006**, *35*, 424. (d) Aguirre-Etcheverry, P.; O'Hare, D. *Chem. Rev.* **2010**, *110*, 4839. (e) Demadis, K. D.; Hartshorn, C. M.; Meyer, T. J. *Chem. Rev.* **2001**, *101*, 2655. (f) Kaim, W.; Klein, A.; Glöckle, M. *Acc. Chem. Res.* **2000**, *33*, 755.

(3) (a) Nemykin, V. N.; Rohde, G. T.; Barrett, C. D.; Hadt, R. G.; Bizzarri, C.; Galloni, P.; Floris, B.; Nowik, I.; Herber, R. H.; Marrani, A. G.; Zanoni, R.; Loim, N. M. *J. Am. Chem. Soc.* **2009**, *131*, 14969. (b) Fox, M. A.; Robert, R. L.; Baines, T. E.; Guennic, B. L.; Halet, J.-F.; Hartl, F.; Yufit, D. S.; Albesa-Jové, D.; Howard, J. A. K.; Low, P. J. *J. Am. Chem. Soc.* **2008**, *130*, 3566. (c) Bonvoisin, J.; Fabre, M. *J. Am. Chem. Soc.* **2007**, *129*, 1434. (d) Semenov, S. N.; Blacque, O.; Fox, T.; Venkatesan, K.; Berke, H. *J. Am. Chem. Soc.* **2010**, *132*, 3115. (e) Vilà, N.; Zhong, Y.-W.; Henderson, J. C.; Abruña, H. D. *Inorg. Chem.* **2010**, *49*, 796. (f) Semenov, S. N.; Taghipourian, S. F.; Blacque, O.; Fox, T.; Venkatesan, K.; Berke, H. *J. Am. Chem. Soc.* **2010**, *132*, 7584. (g) Li, Y.; Joscowicz, M.; Tolbert, L. M. *J. Am. Chem. Soc.* **2010**, *132*, 10374. (h) Hildebrandt, A.; Schaarschmidt, D.; Lang, H. *Organometallics* **2011**, *30*, 556. (i) Kundu, T.; Sarkar, B.; Mondal, T. K.; Fiedler, J.; Mobin, S. M.; Kaim, W.; Lahiri, G. K. *Inorg. Chem.* **2010**, *49*, 6565. (j) Diallo, A. K.; Daran, J.-C.; Varret, F.; Ruiz, J.; Astruc, D. *Angew. Chem., Int. Ed.* **2009**, *48*, 3141. (k) Gao, L.-B.; Kan, J.; Fan, Y.; Zhang, L.-Y.; Liu, S.-H.; Chen, Z.-N. *Inorg. Chem.* **2007**, *46*, 5651.

(4) Robin, M. B.; Day, P. *Adv. Inorg. Chem. Radiochem.* **1967**, *8*, 357.

(5) (a) Mosher, P. J.; Yap, G. P. A.; Crutchley, R. J. *Inorg. Chem.* **2001**, *40*, 1189. (b) Lau, V. C.; Berben, L. A.; Long, J. R. *J. Am. Chem. Soc.* **2002**, *124*, 9042. (c) Das, H. S.; Das, A. K.; Pattacini, R.; Hubner, R.; Sarkar, B.; Braunstein, P. *Chem. Commun.* **2009**, 4387.

(6) (a) Newell, M.; Thomas, J. A. *Dalton Trans.* **2006**, 705. (b) Halpin, Y.; Cleary, L.; Cassidy, L.; Horne, S.; Dini, D.; Browne, W. R.; Vos, J. G. *Dalton Trans.* **2009**, 4146. (c) Slater, J. W.; D'Alessandro, D. M.; Keene, F. R.; Steel, P. J. *Dalton Trans.* **2006**, 1954. (d) Richardson, C.; Fitchett, C. M.; Keene, F. R.; Steel, P. J. *Dalton Trans.* **2008**, 2534. (e) Sarkar, B.; Kaim, W.; Klein, A.; Schwederski, B.; Fiedler, J.; Duboc-Toia, C.; Lahir, G. K. *Inorg. Chem.* **2003**, *42*, 6172. (f) D'Alessandro, D. M.; Dinolfo, P. H.; Davis, M. S.; Hupp, J. T.; Keene, F. R. *Inorg. Chem.* **2006**, *45*, 3261.

(7) (a) Park, J.; Pasupathy, A. N.; Goldsmith, J. I.; Chang, C.; Yaish, Y.; Petta, J. R.; Rinkoski, M.; Sethna, J. P.; Abruña, H. D.; McEuen, P. L.; Ralph, D. C. *Nature* **2002**, *417*, 722. (b) Tang, J.; Wang, Y.; Klare, J. E.; Tulevski, G. S.; Wind, S. J.; Nuckolls, C. *Angew. Chem., Int. Ed.* **2007**, *46*, 3892. (c) Seo, K.; Konchenko, A. V.; Lee, J.; Bang, G. S.; Lee, H. *J. Am. Chem. Soc.* **2008**, *130*, 2553. (d) Flores-Torres, S.; Hutchison, G. R.; Stoltzberg, L. J.; Abruña, H. D. *J. Am. Chem. Soc.* **2006**, *128*, 1513. (e) Zhong, Y.-W.; Vila, N.; Henderson, J. C.; Flores-Torres, S.; Abruña, H. D. *Inorg. Chem.* **2007**, *46*, 10470. (f) Zhong, Y.-W.; Vila, N.; Henderson, J. C.; Abruña, H. D. *Inorg. Chem.* **2009**, *48*, 991.

(8) (a) Zhong, Y.-W.; Wu, S.-H.; Burkhardt, S. E.; Yao, C.-J.; Abruña, H. D. *Inorg. Chem.* **2011**, *50*, 517. (b) Yao, C.-J.; Sui, L.-Z.; Xie, H.-Y.; Xiao, W.-J.; Zhong, Y.-W.; Yao, J. *Inorg. Chem.* **2010**, *49*, 8347. (c) Wu, S.-H.; Burkhardt, S. E.; Yao, J.; Zhong, Y.-W.; Abruña, H. D. *Inorg. Chem.* **2011**, *50*, 3959. (d) Wang, L.; Yang, W.-W.; Zheng, R.-H.; Shi, Q.; Zhong, Y.-W.; Yao, J. *Inorg. Chem.* **2011**, *50*, 7074.

(9) (a) Albrecht, M. *Chem. Rev.* **2010**, *110*, 576. (b) Djukic, J.-P.; Sortais, J.-B.; Barloy, L.; Pfeffer, M. *Eur. J. Inorg. Chem.* **2009**, 817. (c) Jäger, M.; Smeigh, A.; Lombeck, F.; Görls, H.; Collin, J.-P.; Sauvage, J.-P.; Hammarström, L.; Johannsson, O. *Inorg. Chem.* **2010**, *49*, 374. (d) Wadman, S. H.; Lutz, M.; Tooke, D. M.; Spek, A. L.; Hartl, F.; Havenith, R. W. A.; van Klink, G. P. M.; van Koten, G. *Inorg. Chem.* **2009**, *48*, 1887. (e) Duati, M.; Tasca, S.; Lynch, F. C.; Bohlen, H.; Vos, J. G.; Stagni, S.; Ward, M. D. *Inorg. Chem.* **2003**, *42*, 8377. (f) Yang, W.-W.; Wang, L.; Zhong, Y.-W.; Yao, J. *Organometallics* **2011**, *30*, 2236.

(10) (a) Patoux, C.; Launay, J.-P.; Beley, M.; Chodorowski-Kimmers, S.; Collin, J.-P.; James, S.; Sauvage, J.-P. *J. Am. Chem. Soc.* **1998**, *120*, 3717. (b) Fraysse, S.; Coudret, C.; Launay, J.-P. *J. Am. Chem. Soc.* **2003**, *125*, 5880. (c) Sutter, J.-P.; Grove, D. M.; Beley, M.; Collin, J.-P.; Veldman, N.; Spek, A. L.; Sauvage, J.-P.; van Koten, G. *Angew. Chem., Int. Ed.* **1994**, *33*, 1282. (d) Steenwinkel, P.; Grove, D. M.; Veldman, N.; Spek, A. L.; van Koten, G. *Organometallics* **1998**, *17*, 5647.

(11) (a) Nemykin, V. N.; Rohde, G. T.; Barrett, C. D.; Hadt, R. G.; Bizzarri, C.; Galloni, P.; Floris, B.; Nowik, I.; Herber, R. H.; Marrani, A. G.; Zanoni, R.; Loim, N. M. *J. Am. Chem. Soc.* **2009**, *131*, 14969. (b) Wadman, S. H.; Kroom, J. M.; Bakker, K.; Lutz, M.; Spek, A. L.; van Klink, G. P. M.; van Koten, G. *Chem. Commun.* **2007**, 1907. (c) Bomben, P. G.; Koivisto, B. D.; Berlinguette, C. P. *Inorg. Chem.* **2010**, *49*, 4960. (d) Koivisto, B. D.; Robson, K. C. D.; Berlinguette, C. P. *Inorg. Chem.* **2009**, *48*, 9644. (e) Robson, K. C. D.; Koivisto, B. D.; Yella, A.; Sporinova, B.; Nazeeruddin, M. K.; Baumgartner, T.; Gratzel, M.; Berlinguette, C. P. *Inorg. Chem.* **2011**, *50*, 5494.

(12) (a) Ward, M. D.; McCleverty, J. A. *J. Chem. Soc., Dalton Trans.* **2002**, 275. (b) Boyer, J. L.; Rochford, J.; Tsai, M.-K.; Muckerman, J. T.; Fujita, E. *Coord. Chem. Rev.* **2010**, *254*, 309. (c) Lever, A. B. P. *Coord. Chem. Rev.* **2010**, *254*, 1397. (d) Lever, A. B. P.; Gorelsky, S. I. *Struct. Bonding (Berlin)* **2004**, *107*, 77. (e) Dzik, W. I.; van der Vlugt, J. I.; Reek, J. N. H.; de Bruin, B. *Angew. Chem., Int. Ed.* **2011**, *50*, 3356.

(13) Jørgensen, C. K. *Coord. Chem. Rev.* **1966**, *1*, 164.

(14) (a) Das, A. K.; Sarkar, B.; Fiedler, J.; Záliš, S.; Hartenbach, I.; Strobel, S.; Lahiri, G. K.; Kaim, W. *J. Am. Chem. Soc.* **2009**, *131*, 8895. (b) Vasudevan, K. V.; Vargas-Baca, I.; Cowley, A. H. *Angew. Chem., Int. Ed.* **2009**, *48*, 8369. (c) Hübner, R.; Weber, S.; Strobel, S.; Sarkar, B.; Záliš, S.; Kaim, W. *Organometallics* **2011**, *30*, 1414. (d) Poddel'sky, A. I.; Cherkasov, V. K.; Abakumov, G. A. *Coord. Chem. Rev.* **2009**, *253*, 291. (e) Ghumaan, S.; Sarkar, B.; Maji, S.; Puranik, V. G.; Fiedler, J.; Urbanos, F. A.; Jiménez-Aparicio, R.; Kaim, W.; Lahiri, K. *Chem.—Eur. J.* **2008**, *14*, 10816. (f) Deibel, N.; Schweinfurth, D.; Heubner, R.; Braunstein, P.; Sarkar, B. *Dalton Trans.* **2011**, *40*, 431. (g) Kundu, T.; Sarkar, B.; Mondal, T. K.; Mobin, S. M.; Urbanos, F. A.; Fiedler, J.; Jiménez-Aparicio, R.; Kaim, W.; Lahiri, G. K. *Inorg. Chem.* **2011**, *50*, 4753. (h) Das, D.; Mondal, T. K.; Mobin, S. M.; Lahiri, G. K. *Inorg. Chem.* **2009**, *48*, 9800. (i) Meacham, A. P.; Druce, K. L.; Bell, Z. R.; Ward, M. D.; Keister, J. B.; Lever, A. B. P. *Inorg. Chem.* **2003**, *42*, 7887. (j) Remenyi, C.; Kaupp, M. *J. Am. Chem. Soc.* **2005**, *127*, 11399.

(15) (a) Fox, M. A.; Farmer, J. D.; Roberts, R. L.; Humphrey, M. G.; Low, P. J. *Organometallics* **2009**, *28*, 5266. (b) Pevny, F.; Piazza, E. D.; Norel, L.; Drescher, M.; Winter, R. F.; Rigaut, S. *Organometallics* **2010**, *29*, 5912. (c) Olivier, C.; Costuas, K.; Choua, S.; Maurel, V.; Turek, P.; Saillard, J.-Y.; Touchard, D.; Rigaut, S. *J. Am. Chem. Soc.* **2010**, *132*, 5638. (d) Man, W. Y.; Xia, J.-L.; Brown, N. J.; Farmer, J. D.; Yufit, D. S.; Howard, J. A. K.; Liu, S. H.; Low, P. J. *Organometallics* **2011**, *30*, 1852. (e) Gagliardo, M.; Amijs, C. H. M.; Lutz, M.; Spek, A. L.; Havenith, R. W. A.; Hartl, F.; van Klink, G. P. M.; van Koten, G. *Inorg. Chem.* **2007**, *46*, 11133. (f) Pevny, F.; Winter, R. F.; Sarkar, B.; Záliš, S. *Dalton Trans.* **2010**, *39*, 8000. (g) Maurer, J.; Linseis, M.; Sarkar, B.; Schwederski, B.; Niemeyer, M.; Kaim, W.; Záliš, S.; Anson, C.; Zabel, M.; Winter, R. F. *J. Am. Chem. Soc.* **2008**, *130*, 259.

(16) (a) Creutz, C.; Taube, H. *J. Am. Chem. Soc.* **1969**, *91*, 3988. (b) Creutz, C.; Taube, H. *J. Am. Chem. Soc.* **1973**, *95*, 1086.

(17) Fujita, M.; Oka, H.; Ogura, K. *Tetrahedron Lett.* **1995**, *36*, 5247.

(18) (a) D'Alessandro, D. M.; Keene, F. R. *Dalton Trans.* **2004**, 3950. (b) Geiger, W. E.; Barrière, F. *Acc. Chem. Res.* **2010**, *43*, 1030.

(19) (a) Hush, N. S. *Prog. Inorg. Chem.* **1967**, *8*, 391. (b) Hush, N. S. *Electrochim. Acta* **1968**, 1005.

(20) Brunschwig, B. S.; Creutz, C.; Sutin, N. *Chem. Soc. Rev.* **2002**, *31*, 168.

(21) Otón, F.; Ratera, I.; Espinosa, A.; Tárraga, A.; Veciana, J.; Molina, P. *Inorg. Chem.* **2010**, *49*, 3183.

(22) (a) Demadis, K. D.; El-Samanody, E.-S.; Coia, G. M.; Meyer, T. J. *J. Am. Chem. Soc.* **1999**, *121*, 535. (b) Demadis, K. D.; Neyhart, G. A.; Kober, E. M.; White, P. S.; Meyer, T. J. *Inorg. Chem.* **1999**, *38*, 5948. (c) Kober, E. M.; Goldsby, K. A.; Narayana, D. N. S.; Meyer, T. J. *J. Am. Chem. Soc.* **1983**, *105*, 4303.

(23) Rocha, R. C.; Rein, F. N.; Jude, H.; Shreve, A. P.; Concepcion, J. J.; Meyer, T. J. *Angew. Chem., Int. Ed.* **2008**, *47*, 503.

(24) Joss, S.; Reust, H.; Ludi, A. *J. Am. Chem. Soc.* **1981**, *103*, 982.

(25) (a) Maurer, J.; Winter, R. F.; Sarkar, B.; Fiedler, J.; Záliš, S. *Chem. Commun.* **2004**, 1900. (b) Kowalski, K.; Linseis, M.; Winter, R. F.; Zabel, M.; Záliš, S.; Kelm, H.; Krüger, H.-J.; Sarkar, B.; Kaim, W. *Organometallics* **2009**, *28*, 4196. (c) Agarwala, H.; Das, D.; Mobin, S. M.; Mondal, T. K.; Lahiri, G. K. *Inorg. Chim. Acta* **2011**, *374*, 216.

(26) (a) Klamt, A.; Schüürmann, G. *J. Chem. Soc., Perkin Trans. 2* **1993**, 799. (b) Andzelm, J.; Kölmel, C.; Klamt, A. *J. Chem. Phys.* **1995**, *103*, 9312. (c) Barone, V.; Cossi, M. *J. Phys. Chem. A* **1998**, *102*, 1995. (d) Cossi, M.; Rega, N.; Scalmani, G.; Barone, V. *J. Comput. Chem.* **2003**, *24*, 669.

(27) (a) Andrae, D.; Haeussermann, U.; Dolg, M.; Stoll, H.; Preuss, H. *Theor. Chim. Acta* **1990**, *77*, 123. (b) Fuentealba, P.; Preuss, H.; Stoll, H.; Szentpaly, L. V. *Chem. Phys. Lett.* **1989**, *89*, 418.

(28) Stebler, A.; Ammeter, J. H.; Furholz, U.; Ludi, A. *Inorg. Chem.* **1984**, *23*, 2764.

(29) Poppe, J.; Moscherosch, M.; Kaim, W. *Inorg. Chem.* **1993**, *32*, 2640.

(30) Patra, S.; Sarkar, B.; Mobin, S. M.; Kaim, W.; Lahiri, G. K. *Inorg. Chem.* **2003**, *42*, 6469.

(31) (a) Liao, J.; Agustsson, J. S.; Wu, S.; Schönenberger, C.; Calame, M.; Lerous, Y.; Mayor, M.; Jeannin, O.; Ran, Y.-F.; Liu, S.-X.; Decurtins, S. *Nano Lett.* **2010**, *10*, 759. (b) Mahapatro, A. K.; Ying, J.; Ren, T.; Janes, D. B. *Nano Lett.* **2008**, *8*, 2131. (c) Ricci, A. M.; Calvo, E. J.; Martin, S.; Nichlos, R. J. *J. Am. Chem. Soc.* **2010**, *132*, 2494. (d) Leary, E.; Higgins, S. J.; van Zalinge, H.; Haiss, W.; Nichols, R. J.; Nygaard, S.; Jeppesen, J. O.; Ulstrup, J. *J. Am. Chem. Soc.* **2008**, *130*, 12204.

(32) (a) Ren, X.; Alleyne, B. D.; Djurovich, P. I.; Adachi, C.; Tsyba, I.; Bau, R.; Thompson, M. E. *Inorg. Chem.* **2004**, *43*, 1697. (b) Ma, B.; Kim, B. J.; Poulsen, D. A.; Pastine, S. J.; Fréchet, J. M. J. *Adv. Funct. Mater.* **2009**, *19*, 1024.

(33) Garcia-Canadas, J.; Meacham, A. P.; Peter, L. M.; Ward, M. D. *Angew. Chem., Int. Ed.* **2003**, *42*, 3011.

(34) (a) Becke, A. D. *J. Chem. Phys.* **1993**, *98*, 5648. (b) Lee, C.; Yang, W.; Parr, R. G. *Phys. Rev. B* **1988**, *37*, 785.

(35) Frisch, M. J. et al. *Gaussian 03*, revision E.01; Gaussian Inc.: Pittsburgh, PA, 2007. The full list of authors is provided in the Supporting Information.

(36) (a) Dunning, T. H.; Hay, P. J. In *Modern Theoretical Chemistry*; Schaefer, H. F., Ed.; Plenum: New York, 1976; Vol. 3, p 1. (b) Hay, P. J.; Wadt, W. R. *J. Chem. Phys.* **1985**, *82*, 270. (c) Wadt, W. R.; Hay, P. J. *J. Chem. Phys.* **1985**, *82*, 284. (d) Hay, P. J.; Wadt, W. R. *J. Chem. Phys.* **1985**, *82*, 299.